Investigating optimal cutting configurations for the contour method of weld residual stress measurement

Accepted Manuscript

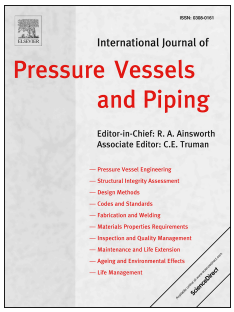

Investigating optimal cutting configurations for the contour method of weld residual stress measurement

O. Muránsky, F. Hosseinzadeh, C.J. Hamelin, Y. Traore, P. Bendeich

PII: S0308-0161(16)30073-4

DOI: 10.1016/j.ijpvp.2017.04.006

Reference: IPVP 3609

To appear in: *International Journal of Pressure Vessels and Piping*

Received Date: 19 February 2016

Revised Date: 18 January 2017

Accepted Date: 4 April 2017

Please cite this article as: Muránsky O, Hosseinzadeh F, Hamelin CJ, Traore Y, Bendeich P, Investigating optimal cutting configurations for the contour method of weld residual stress measurement, *International Journal of Pressure Vessels and Piping* (2017), doi: 10.1016/j.ijpvp.2017.04.006.

Investigating Optimal Cutting Configurations for the Contour Method of Weld Residual Stress Measurement

O. Muránsky [1], F. Hosseinzadeh [2], C.J. Hamelin [1], Y. Traore [2], P. Bendeich [1]

[1] ANSTO, Institute of Materials Engineering, Lucas Heights, NSW, Australia

[2] The Open University, Materials Engineering, Milton Keynes, MK7 6AA, UK

Abstract

The present work examines optimal cutting configurations for the measurement of weld residual stresses (WRS) using the contour method. The accuracy of a conventional, single-cut configuration that employs rigid clamping is compared with novel, double-embedded cutting configurations that rely on specimen self-constraint during cutting. Numerical analyses examine the redistribution of WRS and the development of cutting-induced plasticity (CIP) in a three-pass austenitic slot weld (NeT TG4) during the cutting procedure for each configuration. Stress intensity factor (SIF) analyses are first used as a screening tool; these analyses characterise lower stress intensities near the cutting surface when double-embedded cutting configurations are used, relative to SIF profiles from a single-cut process. The lower stress intensities indicate the development of CIP – which will ultimately affect back-calculated WRS – is less likely to occur when using an embedded configuration. The improvements observed for embedded cutting approaches are confirmed using three-dimensional finite element (FE) cutting simulations. The simulations reveal significant localised plasticity that forms in the material ligaments located between the pilot holes and the outer edges of the specimen. This plasticity is caused by WRS redistribution during the cutting process. The compressive plasticity in these material ligaments is shown to reduce the overall tensile WRS near the weld region before this region is sectioned, thereby significantly reducing the amount of CIP when cutting through the weld region at a later stage of the cutting procedure. Further improvements to the embedded cutting configuration are observed when the equilibrating compressive stresses in material ligaments are removed entirely (via sectioning) prior to sectioning of the high WRS region in the vicinity of the weld. All numerical results are validated against a series of WRS measurements performed using the contour method on a set of NeT TG4 benchmark weld specimens.

Keywords: Contour method; Finite element modelling; Residual stress; Welding.

1. Introduction

Residual stresses are self-equilibrating stresses locked in a component or engineering structure in the absence of an external load. Weld residual stresses (WRS) arise as a result of *shape misfits* [1] between different regions of the weldment, caused by heterogeneous plastic deformation during the welding process. WRS can *add to* or *subtract from* operational stresses, and can thus lead to an unexpected overload and premature failure of a component. For instance, it is well understood that WRS plays a significant role in crack initiation and growth by providing the driving force for damage evolution [1]. It is therefore of technological importance to account for the magnitude and distribution of WRS in structural integrity assessments.

A number of non-destructive[1] (diffraction) and destructive[1] (stress-relief) techniques for residual stress measurement are well established and readily available. Diffraction techniques might seem preferable as they allow measurement of more than one stress tensor component within the sample without affecting the integrity of the specimen under investigation. However, a number of limitations inherent to both neutron and synchrotron diffraction techniques exist: (i) the maximum allowable specimen thickness is limited by the beam absorption in a given material; (ii) the spatial resolution is limited by the beam size and the grain size of the material (<150 μm); (iii) stress-free[2] reference specimens of the weld and parent materials are often required; (iv) the cost associated with the diffraction-based measurement is high; and (v) diffraction equipment is not readily available. As a result, stress-relief techniques (e.g. the contour method [2], slitting [3], deep-hole drilling [4] and hybrid techniques [5, 6]) are often an attractive alternative [7], particularly for industrial applications.

One of the most popular destructive (stress-relief) techniques for residual stress measurement is the contour method [2, 8-10], which is based on a variation of Bueckner's principle [11] of elastic superposition. The contour method is performed in four stages: (i) cutting the component along the plane-of-interest using electric discharge machining (EDM); (ii) measuring the resultant out-of-plane displacement (OoPD) caused by stress relief, often using a coordinate measuring machine (CMM); (iii) post-processing of the measured OoPD data to eliminate artefacts and noise introduced in the EDM cutting process; and (iv) back-calculation of the original (pre-cut) residual stresses using a fully elastic finite element (FE) analysis. An obvious limitation of the traditional contour method is that only one component of residual stress can be determined per cut, i.e. perpendicular to the plane-of-cut. On the other hand, the contour method is insensitive to microstructure variation (weld/parent metal), the sample thickness, and furthermore required equipment is readily available.

While the contour method for residual stress measurement is straightforward in principle, it relies on a number of theoretical assumptions [8, 12] that may lead to inaccuracies in recovered (back-calculated) residual stresses. Hence, when measuring residual stresses using the contour method, one needs considering the effect of both *anti-symmetric* and *symmetric* errors [12]. Anti-symmetric errors introduce asymmetry in what should otherwise be symmetric OoPD (i.e. the recorded OoPD profile on one side of the cut should be a mirror image of OoPD profile on the opposite side of the cut). These errors are caused by shear stresses, crooked cutting, or artefacts introduced by the EDM cutting process, and can be easily removed in post-processing by averaging the measured OoPD on both sides of the cut [12]. Symmetric errors can be separated into two categories: errors dependent on the internal stress state of the component (i.e.

[1] The original internal residual stress field in the specimen is preserved during the measurement process. However, the extraction of a reference stress-free coupon from another specimen is often required.

[2] The stress-free lattice spacing is essential for diffraction-based stress measurements in order to calculate corresponding elastic lattice strains, which can then be used in stress calculations using Hooke's law.

magnitude of residual stresses); and errors that are independent of the stress state. Symmetric errors that *do not* depend on the stress state within the component can be either prevented [13-16] or corrected by performing a stress-free cut to quantify the error, which can be then simply subtracted from the contour measurements in post-processing stage [2, 10, 12, 17-20]. In contrast, symmetric errors that *depend* on the internal stress state within the component - (i) cutting-induced plasticity (CIP) error [21-24] and so-called (ii) bulge [12] - cannot be readily corrected after the cut is performed, thus they need to be prevented or at least minimised during the contour cutting process. It is of technological importance to minimize the effect of these errors, because of their significant effect on the accuracy of the contour method for stress measurement. CIP is traditionally minimised through the use of significant mechanical restraint (clamping) on either side of the plane-of-cut during the cutting process. However, because such rigid clamping is hard to achieve in practice, recent work focuses on alternative cutting strategies that do not rely on specimen clamping.

The present study explores the potential of embedded cutting configurations in controlling CIP when applying the contour method to WRS measurements. This study focuses on the measurement of WRS in a three-pass austenitic steel slot weld specimen, designated NeT TG4 [25]. A conventional single-cut configuration with rigid clamping is compared with double-embedded cutting configurations, which rely on self-constraint of the specimen during the cutting process. The following cutting configurations are examined: (i) a conventional (1-Cut) configuration with rigid clamping; (ii) a 4-Cut double-embedded configuration with no clamping[3]; and (iii) a 5-Cut double-embedded configuration with no clamping. Detailed information regarding each strategy is provided in Section 3. The efficacy of these contour cutting configurations in mitigating the effects of CIP (and consequently on the accuracy of the measured WRS) is compared numerically using validated finite element (FE) simulations and fracture mechanics analyses. These numerical solutions are then validated experimentally using contour cutting measurements.

2. The NeT TG4 benchmark weld specimen

A Task Group (TG4) has been established by the European Network on Neutron Techniques Standardisation for Structural Integrity (NeT) to examine WRS in a three-pass austenitic steel weld, and provide best-practice guidelines for the measurement and numerical prediction of WRS. A series of benchmark weld specimens were manufactured under the auspices of NeT TG4. The weld design comprises a three-pass ER316L austenitic steel slot weld in solution heat-treated AISI 316LN austenitic steel plate. The nominal dimensions of the plate, shown in Fig. 1, are 150(X) $\times$ 18(Y) $\times$ 194(Z) mm^3 with an 80-mm long and 6-mm deep centreline slot. The slot was filled with three superimposed weld passes via a mechanised tungsten inert gas (TIG) welding process to ensure welding process repeatability. These benchmark specimens were used in two ways: (i) WRS measurements were conducted using a variety of complementary techniques, allowing the development of best-practice measurement guidelines; and (ii) process variables (welding current, voltage, torch speed, etc.) from the benchmark problem were used as input data to develop physically-based FE welding simulations. The WRS predicted from these simulations were then validated against the WRS measurements, thus providing an opportunity to identify best practise for accurate welding simulation. The following sections highlight pertinent details of both

[3] While no significant mechanical restraint is provided, rigid body rotation is prevented during the numerical analysis. In reality, this rotation would be prevented by light clamping.

the diffraction measurement and modelling efforts; the reader is directed to Ref. [25, 26] should a more comprehensive review of each procedure be desired.

2.1 WRS measurement

Neutron diffraction measurements were carried out using the KOWARI diffractometer at the Australian Nuclear Science and Technology Organisation (ANSTO) [25]. A gauge volume of ($2 \times 2 \times 2$) mm^3 was defined using primary and secondary sets of cadmium slits. The specimen was rocked (±)5° during the measurement to increase grain statistics since coarse grains were present in the weldment, particularly within the weld region. Diffraction measurements of residual stress are based on the measurement of residual elastic strains in at least two orthogonal sample directions (principal axes). In the present study, elastic residual strains in three principal directions (X = transverse, Y = normal, Z = longitudinal) were determined from the relative shift in the position of the {311} diffraction peak, from its position within the final post-weld specimen to its position within a stress-free coupon. The {311} reflection was chosen because intragranular (Type II) stresses have the smallest influence on strain measurements taken for this reflection [27]. The measured residual elastic strains were then used to calculate residual stresses via Hooke's law, employing the following elastic diffraction constants [28]: E^{311} = 183.6 GPa; ν^{311} = 0.306. Longitudinal (Z) WRS profiles measured along lines B2 and B16 (Fig. 1) are shown in Figs. 2a and 2b, respectively. The B2 line passes through the last of the three deposited weld beads. The B16 line does not pass through weld metal but instead through the adjacent parent metal, which has experienced welding-induced cyclic loading.

Synchrotron diffraction measurements were carried out using the ID15A beamline at the European Synchrotron Radiation Facility (ESRF) [26]. Monochromatic high-energy synchrotron radiation with a wavelength of 0.0114 nm was focussed with Compound Refractive Lenses (CRLs) to a beam size of 14 µm x 14 µm. The spiral slit technique [29] was used to obtain a depth and phase[4] resolved diffraction signal. To enhance the measurement statistics, the specimen was oscillated along the sample Z direction (ΔZ = 4 mm). Due to the coarse-grain microstructure, the resulting spotty diffraction patterns were subjected to a novel data analysis procedure [30] to determine the elastic residual strains. Rather than performing a powder-like analysis with the fitting of diffraction peaks, a procedure based on the centre-of-mass position of diffraction spots from individual grains was applied [26]. The diffraction spots of {111}, {220}, {311}, and {222} reflections were used to derive residual elastic strains, which were then used in the residual stress calculation (Hooke's law) employing the same elastic diffraction constants as in the neutron diffraction analysis. Unlike in neutron diffraction measurements, synchrotron diffraction only allows measurement of transverse (X) and longitudinal (Z) residual strain components. Hence, the residual stress calculation was based on a biaxial stress-state assumption, i.e. plane stress was assumed in the normal (Y) direction. Synchrotron diffraction measurements of longitudinal WRS profiles are shown alongside the neutron diffraction measurements in Figs. 2a and 2b. Good agreement between independent diffraction techniques was achieved, thus validating the plane-stress assumption used in synchrotron measurements. In addition to WRS profiles, the high spatial resolution and short data acquisition times of the synchrotron diffraction technique allowed for the construction of 2D stress maps. Longitudinal WRS along the plane-of-cut (plane B, Fig. 1), comprising of 246 individual measurements, is presented in Fig. 2c.

[4] Note that an elevated Cr content in the filler material causes stabilization of δ-ferrite (~5% by volume); this δ-ferrite was neglected in both diffraction measurements and FE simulations.

2.2 WRS prediction

The WRS in the NeT TG4 weld specimens have been predicted via welding simulations developed using the ABAQUS commercial FE package [31-33]. A 3D half-model comprising of 38,220 hexahedral quadratic elements (schematically shown in Fig. 1) was used to take advantage of specimen and process symmetry about the weld centreline, improving computational efficiency. A sequentially coupled thermo-mechanical FE simulation was performed, whereby the numerical solution from the thermal FE analysis was used as an input for the mechanical FE analysis. Thermal analyses use quadratic heat transfer elements (ABAQUS designation DC3D20) while mechanical analyses use reduced-integration quadratic stress elements (ABAQUS designation C3D20R).

A dedicated welding heat-source modelling tool (FEAT-WMT) [34] was used to calibrate an ellipsoidal Gaussian volumetric heat source. Calibration was performed using cross-weld fusion boundary information, as well as thermocouple data acquired whilst welding the NeT TG4 specimens [25]. Once the heat source was calibrated, the transient thermal solution was supplied from FEAT-WMT to ABAQUS in the form of time- and spatially-resolved volumetric power density data (via the ABAQUS DFLUX subroutine). The mechanical analysis employed a Lemaitre-Chaboche isotropic-kinematic plasticity model [35] to accurately capture the welding-induced cyclic hardening of 316LN alloy during the welding process. Sensitivity analyses [31] revealed that use of an isotropic-kinematic (mixed) cyclic hardening model results in the most accurate prediction of WRS and welding-induced plasticity (WIP) [36]. High-temperature annealing (i.e. the loss of accumulated isotropic plasticity at high temperatures) was controlled via a two-stage annealing functionality developed for ABAQUS [37]. While the annealing behaviour may not significantly affect WRS predictions, it does affect predictions of WIP [36] that are used in damage assessments.

Figure 2 highlights the agreement between the numerical WRS solution from the welding simulation and both sets of diffraction measurements. Cross-weld longitudinal WRS predictions along lines B2 and B16 are presented in Figs. 2a and 2b respectively, alongside diffraction results. A two-dimensional contour plot of predicted longitudinal WRS along the B plane is shown in Fig. 2d for direct comparison against the synchrotron-measured results shown in Fig. 2c. It is clear that quantitative accuracy in the predicted WRS distribution was achieved relative to the complementary diffraction measurements taken, thus validating the numerical welding simulation [25, 31]. Such validation is important for the present contour cutting analyses, as this FE solution is used as model input for the contour cutting simulations.

3. Cutting configurations

The present study examines the effect of three different cutting configurations on the accuracy of the contour method for residual stress measurement in the NeT TG4 benchmark specimen. These configurations are shown schematically in Fig. 3. The first configuration (Fig. 3a) represents a conventional (1-Cut) approach to the contour method, where a single cut is progressed from the one edge of the specimen to the other. The direction of EDM wire travel is in the transverse (X) direction. In this approach, WRS redistribution occurs predominantly near the cut tip as the stresses behind the cut relax, leading to stress intensification ahead of the cut and the possibility of cutting-induced plasticity (CIP). To mitigate CIP, mechanical restraint (i.e. clamping) is often applied to control WRS redistribution during the cutting process, thereby limiting CIP. The clamps for this 1-Cut configuration have been placed towards the outer edges of the specimen. It should be noted that the most effective clamping is applied closest to the plane-of-cut; however, weld and sample geometries often prevent external clamping at these locations.

Unlike the 1-Cut configuration, embedded configurations provide self-constraint and thus "internal clamping" of the specimen. These configurations can be used to control and/or redirect WRS redistribution away from the region of interest (e.g. weld region) during the cutting process. Figure 3b presents a 4-Cut, double-embedded[5] cutting configuration. The first cut (Cut-1) is progressed from Pilot Hole 1 (PH1) towards the weld region, and is terminated once the cut has passed through the weld fusion zone (cut length = 75 mm). The second cut (Cut-2) progresses from Pilot Hole 2 (PH2), and terminates once the end of Cut-1 is reached (cut length = 65 mm). Finally, Cut-3 and Cut-4 are used to sever the material ligaments remaining near the sample edges. This double-embedded configuration has been shown to significantly reduce the effect of CIP and thus improve the accuracy of recovered WRS [38, 39].

The 5-Cut double-embedded configuration (Fig. 3c) is similar to the 4-Cut configuration, with some minor but important distinctions that are believed to further improve the accuracy of WRS measurements. Firstly, both Cut-1 and Cut-2 approach the weld region, which is region of interest; however, neither of these cuts pass through the weld region. Cut-3 and Cut-4 are then applied to sever the outer material ligaments, which were used for specimen self-constraint, see Fig. 3c. These material ligaments contain the equilibrating compressive stresses in the specimen (see below). By releasing these compressive stresses, the redistribution of internal WRS leads to reduction of the high tensile WRS in the weld region (region of interest) – only the variation in WRS across the weld region causes some internal stresses to remain. Consequently, it is believed that the propensity for CIP when cutting through the weld region (Cut-5) can further reduced.

Complementary numerical analyses and experimental measurements are carried out to examine the efficacy of these three contour cutting configurations in minimizing the effects of CIP and thus improving contour method accuracy. The answers to two questions are sought in the present work:

(Q1): How well do embedded cutting configurations (4-Cut, 5-Cut), which are not subject to external mechanical restraint, perform relative to conventional (1-Cut) configurations with applied clamping?

(Q2): What improvements are gained by releasing the outer equilibrating stresses prior to sectioning the weld region in an embedded cutting configuration? That is, does a 5-Cut configuration perform significantly better than its 4-Cut counterpart?

4. Numerical analyses

4.1 SIF analysis of contour cutting

The EDM cutting process used for the contour method is analogous to the propagation of a full-penetration crack across the specimen plane-of-cut. As such, the severity of stress concentrations caused by stress redistribution near the leading edge of the cut (or "cut tip") can be estimated by calculating the mode I stress intensity factor (SIF) K_I at this position [40-42]. By having prior knowledge of the residual stress distribution in a specimen, a fully elastic FE simulation of the cutting process can be performed and linear elastic fracture mechanics (LEFM) used to calculate K_I at the cut tip. By plotting K_I as a function of cut tip location along the plane-of-cut, the analyst can observe the severity of stress intensification expected during the cutting process and ultimately the likelihood of CIP. These analyses are less computationally expensive

[5] The term "double-embedded" refers to the fact that two pilot holes have been drilled near the outer edges of the sample, and two embedded cuts are progressed from each of these pilot holes toward the weld region.

relative to three-dimensional FE contour cutting simulations due to three simplifications: (i) a two-dimensional idealisation is made of the WRS distribution in the sample; (ii) only the initial WRS along the plane-of-cut is required; and (iii) symmetry is assumed across the plane-of-cut. This latter simplification is useful because it allows the cutting process to be simulated through the incremental removal of a symmetry boundary condition located along the plane-of-cut of the FE half-model. A SIF analysis can thus be used for rapid assessment of a potential cutting configuration, making it a valuable screening tool for cutting process optimization.

In the present work, SIF analyses of each cutting configuration (Fig. 3) were performed using the ABAQUS commercial FE package [37]. The 2D FE mesh comprised 4-node bilinear elements with reduced integration and hourglass control (ABAQUS designation CPS4R). A non-uniform mesh was used; near the vicinity of the cut tip, a relatively fine mesh of 0.4 x 0.4 mm^2 elements was defined to capture the large stress gradients expected in this region. Cutting was simulated by the incremental release of the symmetry boundary condition used to constrain the plane-of-cut. Simultaneously, stresses were applied along the newly created cut faces [40, 41]; these stresses represent the inverse of the WRS distribution in the NeT TG4 specimen at each point along the cut face. The longitudinal (Z) WRS measured along the B2 line using neutron diffraction (Fig. 2a) was used for this idealized 2D stress state; this line profile was chosen as it provides the most representative cross-weld WRS distribution from the measured data set. The application of these inverse stresses to a stress-free model is an extension of Bueckner's principle of elastic superposition [43], which forms the basis of residual stress recovery using the contour method. As the contour cut progresses across the weld specimen, the SIF values at the cut tip are recorded. The resultant SIF profiles can be then used to examine regions where CIP is likely to occur during the cutting process.

4.2 3D cutting simulations

While the simplifications used in SIF analyses provide an efficient means of optimising the cutting process, more accurate predictive capabilities are used to directly quantify the magnitude of CIP across the plane-of-cut for a given cutting configuration. Greater predictive capability may be required for thick-section multi-pass welds since the two-dimensional simplifications of a SIF analysis – which assume a uniform WRS profile exists across the sample thickness – may not accurately capture through-thickness WRS variations. Three-dimensional FE cutting simulations containing the full WRS distribution of the sample are therefore used to predict CIP across the plane-of-cut.

Elasto-plastic FE models were developed to simulate the cutting process and determine the extent of CIP for a given cutting configuration. While the SIF analyses used the neutron measured WRS profile along B2 line as the reference stress state, the 3D contour cutting simulations used full tensor values of WRS and WIP distributions across the entire NeT TG4 specimen. These distributions were obtained using the validated weld simulation for NeT TG4 [25]. All relevant data (post-weld residual stresses, plastic strains) was transferred from the FE weld model to the FE cutting model, which has a different FE mesh and set of boundary conditions dependent on the configuration analysed (Fig. 3). It should be noted that both the magnitude and direction of the accumulated plastic strain and associated backstress tensor from welding are captured, as Bauschinger effects must also be considered for the subsequent cutting process. As mentioned, both weld and parent metals use a Lematire-Chaboche cyclic work hardening model [35] to account for such effects. Prior to data transfer, the welding-induced distortion was omitted from the analysis in order to simplify the cutting model geometry. This omission was achieved by running an additional mechanical analysis step after the weld simulation wherein the nodal displacements were not recorded, thus removing all welding-induced distortion information. It

has been confirmed that the omission of the welding-induced distortion has a negligible effect on the magnitude and distribution of the predicted WRS and WIP [44]. The results of the symmetric welding solution was then mirrored about the symmetry plane (plane D in Fig. 1) and mapped onto the cutting models.

Optimization of the cutting model focused on significant FE mesh refinement near the plane-of-cut to accurately capture the redistribution of WRS and the evolution of CIP during the cutting process. Even though the element type for the cutting simulation is the same as that used for the mechanical weld analysis (ABAQUS designation C3D20R), the number of elements increased from 38,220 to 396,626. The contour cutting process was simulated by successive removal of through-thickness vertical element sets[6] measuring $0.32(X) \times 18(Y) \times 0.32(Z)$ mm^3 (schematically shown in Fig. 1) with an advance rate of one element set per second. Note that these numerical analyses are time-independent and the time step was arbitrarily chosen as one second. After completion of the cutting simulation, the OoPD of nodes on both sides of the cut (i.e. both cut surfaces) was obtained and used to back-calculate the original (pre-cut) distribution of WRS using a fully elastic stress analysis. This procedure is identical to that used when back-calculating WRS using experimental data (Section 6). In addition, CIP was directly calculated across the cut surface for each cutting configuration. This calculation was performed by taking the post-cut longitudinal plastic strain at each nodal point on the cut surface, and subtracting the pre-cut longitudinal component of WIP from this amount. Both the back-calculated WRS and predicted CIP are then used to compare the efficacy of each cutting configuration in limiting the adverse effects of CIP on the contour method.

5. Numerical results

5.1 Relative probability assessment of CIP via SIF analysis

Figure 4 compares the variation of SIF as function of the cut length along the plane-of-cut for both embedded contour cutting configurations (4-Cut, 5-Cut) with the conventional single-cut configuration (1-Cut). In the case of double-embedded configurations, the SIF values are reported for the moving as well as stationary tips. These stationary tips are created at the pilot holes (PH1, PH2) and at the cut stops (the end of Cut-1 for the 4-Cut configuration, and the ends of Cut-1 and Cut-2 for the 5-Cut configuration, see Fig. 3).

Let us first examine the SIF distribution for the conventional 1-Cut contour cutting configuration so a direct comparison with the embedded contour cutting configurations can be made. Two extrema in the 1-Cut SIF profile (Fig. 4) can be observed: (i) -55 MPa$\sqrt{m}$ at X = -50 mm, suggesting that the release of equilibrating compressive WRS (Z) outside of the weld region (see Fig. 2) might result in compressive CIP in this region; and (ii) +60 MPa$\sqrt{m}$ at X = +15 mm, indicating the likelihood of tensile CIP when cutting through the tensile WRS region near the weld. By comparing the 1-Cut SIF profile with both embedded-configuration SIF profiles in Fig. 4, it becomes clear that embedded configurations reduce the magnitude of the compressive SIF at the beginning of the contour cutting process. This improvement is more pronounced in the 5-Cut configuration (Fig. 4b) relative to the 4-Cut counterpart (Fig.4a). Hence, there is a lower probability for CIP to occur in this region in double-embedded configurations, relative to the 1-Cut configuration. The global extrema in 4-Cut and 5-Cut SIF distributions are observed in different parts of the specimen during cutting. For the 4-Cut configuration a tensile extremum is observed

[6] The size of the removed element set is based on the EDM wire diameter (0.25mm) used in the experiments. The width of cut also accounts for the material evaporated around the wire during cutting.

at X = +5 mm (+51 MPa√m), in the weld region where the Cut-1 meets Cut-2. For the 5-Cut configuration a compressive extremum is observed at X = +15 mm (-52 MPa√m), as Cut-5 approaches the end of Cut-2. These results suggest the greatest likelihood of CIP when using an embedded cutting configuration exists in these regions; however, this likelihood is smaller than that observed for conventional single-cut configurations. It is further important to point out the high SIF values present in both embedded cutting configurations located near the stationary tips, which suggest a high probability for CIP to develop close to both pilot holes, and near cut ends. Such a finding implies any cutting configuration should be planned such that pilot holes and cut ends should be located outside any regions of interest (e.g. the near-weld region).

The results of these SIF analyses help to answer the first question that forms the basis of this work:

How well do embedded cutting configurations (4-Cut, 5-Cut), which are not subject to external mechanical restraint, perform relative to conventional (1-Cut) configurations with applied clamping?

Comparison of SIF profiles in the 4-Cut and 5-Cut configurations relative to the 1-Cut configuration shows a reduction in stress extrema, which confirms these embedded strategies are less likely to produce CIP and thus lead to more accurate WRS measurements. It is evident that the WRS within the released material of an embedded cut is redistributed to two functional locations (i.e. either end of the embedded cut), while conventional cuts only have one functional location for WRS redistribution (i.e. the leading cut tip). Further optimization of these cutting configurations (e.g. pilot hole location, cut length, etc.) can be performed using parametric SIF analyses.

5.2 Quantitative and qualitative assessment of CIP via FE simulations

SIF analyses have confirmed the stress intensification present when using a conventional single-cut (1-Cut) configuration is greater than that calculated for double-embedded cutting configurations (4-Cut, 5-Cut). This intensification will often lead to the development of CIP in the material, which will consequently affect the measured OoPD and ultimately the accuracy of the back-calculated WRS across the plane-of-cut. The following numerical analyses will quantify the improvement of 4-Cut and 5-Cut configurations relative to the 1-Cut approach. Quantification is carried out through direct comparison of the predicted CIP across the plane-of-cut for each cutting configuration; predicted CIP for each configuration is presented in Fig. 5(a-c). Note that all configurations predict levels of CIP that are greater than the original WIP distributions predicted along the NeT TG4 plane-of-cut (Fig. 5d). Of the three approaches, the 5-Cut configuration (Fig. 5c) has the lowest CIP extrema. While the 4-Cut extrema (Fig. 5b) are greater than those predicted for the 1-Cut approach (Fig. 5a), it is evident these extrema are highly localized in the outer material ligaments formed between the pilot holes and the edge of the specimen, near the stationary cut tips, which SIF have confirmed to be regions of high K_I. However, *the magnitude of CIP alone will not dictate the overall influence it has on accuracy of back-calculated WRS*; the location and distribution of CIP is also an important feature. Figure 5(e-g) presents the back-calculated longitudinal (Z) WRS profiles obtained using the predicted OoPD data (Fig. 6) from each cutting simulation. When comparing these results against the initial (pre-cut) WRS profile taken along the plane-of-cut (Fig. 5h), it is evident that the highly localised nature of CIP in the outer material ligaments when using embedded cutting configuration (Fig. 5b,c) have little influence on the overall accuracy of the corresponding back-calculated WRS distribution (Fig. 5f) relative to the WRS profile recovered using the 1-Cut approach (Fig. 5e). The WRS contours recovered using both

embedded configurations more closely represent the original longitudinal WRS distribution, thereby confirming the qualitative assessment performed via SIF analysis.

To further elucidate the effect of CIP on the accuracy of WRS back-calculation, it is useful to examine the predicted OoPD profiles for each cutting configuration. Figure 6 compares the predicted OoPD across the plane-of-cut using elasto-plastic FE simulations against those obtained from idealized, fully elastic FE simulations that will not produce CIP[7]. Note that greater agreement between the elasto-plastic OoPD profile and the idealized fully elastic OoPD profile leads to greater accuracy in the back-calculated WRS. Figure 6a shows us that even though the 1-Cut configuration produces a relatively small amount of CIP (Fig. 5a), the contribution of this CIP to the OoPD is significant as evidenced by the deviations in the elasto-plastic OoPD profile relative to the fully elastic prediction. The situation is different in both embedded cutting configurations (Figs. 6b,c), which effectively localise CIP (to roughly -7% strain) within narrow ligaments formed beyond the pilot holes on both sides of the specimen (see appendix). The OoPD data obtained beyond the pilot holes (X < -5 mm, X > +70 mm) are completely removed from the subsequent WRS back-calculation in embedded cutting simulations, leading to a loss of usable data in these regions.

In the case of the 4-Cut configuration (Fig. 6b), significant localisation (roughly +4% strain) is also observed within the region where Cut-2 approaches the end of Cut-1. In contrast, a similar localization is not observed in the predicted 5-Cut OoPD data (Fig. 6c). This leads us to the second question that forms the basis of this work:

What improvements are gained by releasing the outer equilibrating stresses prior to sectioning the weld region in an embedded cutting configuration? That is, does a 5-Cut configuration perform significantly better than its 4-Cut counterpart?

As discussed above, it is evident from the back-calculated WRS shown in Fig. 5(e-g) that the 5-Cut configuration leads to the most accurate back-calculated WRS in the region of interest (i.e. the near-weld region). However, to gain a deeper understanding of why the 5-Cut configuration seems to be more effective in eliminating the effects of CIP when compared to the 4-Cut configuration, it is necessary to look into the redistribution of WRS and evolution of CIP during the contour cutting process for both configurations. Figure 7 presents the predicted redistribution of WRS and the associated development of CIP along the B9 line (Fig. 1), as a function of cutting progress. One can directly observe the redistribution of WRS during the cutting process that leads to stress concentrations at the cut tips. From Fig. 7 it is clear that both embedded cutting configurations effectively direct the CIP to the outer material ligaments located beyond the pilot holes. As compressive WRS continue to accumulate in these ligaments, they ultimately cause the material to yield; this trend is supported by the high levels of compressive CIP within the ligaments as shown in Figs. 5(b,c). The main difference between the 4-Cut and 5-Cut configurations lies in the way they deal with high tensile stresses in the weld region. The proposed benefit of the 5-Cut configuration is to first relieve the high tensile WRS located in the weld region as much as possible before cutting through it. This relaxation is achieved by first removing the material ligaments beyond the pilot holes (Cut-3, Cut-4), which contain equilibrating compressive stresses. Figure 7b shows the relaxation in tensile WRS within the near-weld region between the “Cut-2 Stop” line and “Cut-4 Stop” line. As a result, the ligament formed when Cut-5

[7] Since a fully elastic cutting simulation will produce no CIP, the resultant back-calculated WRS distribution will be identical to the original (pre-cut) WRS. As a result, the fully elastic OoPD results presented in Fig. 6 are identical regardless of cutting configuration.

approaches the end of Cut-2 does not contain significant WRS intensification, and CIP is notably lower than what is predicted for the 4-Cut configuration (Fig. 7a).

While the 5-Cut approach is more effective at mitigating CIP, there are ways of improving the 4-Cut results that largely circumvent these plasticity errors. Improvements come largely from data filtering. For example, the OoPD data in the near-weld region that was affected by CIP in the 4-Cut approach (the shaded region in Fig. 6b) was removed when back-calculating WRS. This data was replaced by an interpolated dataset to produce the back-calculated WRS profile shown in Fig. 5f. Note that this data filtering could only be performed since we are aware of the significant CIP that accumulates in this region; in reality – when the analyst does not have the luxury of a well-characterised benchmark specimen – it may not be possible to identify data affected by CIP. Regardless, it appears the use of pilot holes provides the greatest improvement of measurement accuracy in double-embedded cutting configurations; however, care must be taken to ensure the ligaments formed between the pilot holes and the outer edges of the sample are of a size suitable to mitigate plasticity in the region of interest (i.e. the weld region). A parametric study illustrating the selection of optimal pilot-hole locations is appended (see appendix).

6. Experimental validation

To check the validity of the present numerical analyses, two nominally identical NeT TG4 weld specimens were experimentally sectioned using the 4-Cut and 5-Cut configurations. The specimens were sectioned at specimen mid-length along the transverse plane to recover the longitudinal component of WRS, based on the measured OoPD across the plane-of-cut. To implement these double-embedded cutting configurations, two 1.8-mm diameter pilot holes were drilled at a 5 mm transverse offset distance from each of the specimen edges (schematically shown in Fig. 3). EDM-induced cutting artefacts close to the surfaces of the specimen were prevented by bonding sacrificial layers of stainless steel on the top and back faces of the weld specimen [13, 14]. In addition, finger clamps were used to prevent the specimen moving on the EDM table during cutting. Note that the sacrificial layers and the finger clamps were omitted from the contour cutting simulations present above (though rigid-body motion is prevented in the FE models).

After the cutting was completed, a Zeiss Eclipse CMM fitted with a Micro-Epsilon triangulating laser probe and a 4-mm diameter ruby-tipped Renishaw PH10M touch trigger probe was used for contour measurement of the cut surfaces. First the perimeter of the surface was measured with the touch probe using a 2-mm pitch, and then the OoPD in the longitudinal (Z) direction was measured using the triangulating laser sensor on a (0.125×0.125) mm grid. The as-measured OoPD profiles for the 4-Cut and 5-Cut configurations are shown in Figs. 6d and 6e, respectively. As-measured OoPD data were then processed using the standard approach described in Refs. [45, 46] to remove asymmetric errors and signal noise. In addition, the OoPD measurements strongly affected by CIP were removed in a manner similar to that used for the predicted OoPD data: (i) the measured OoPD data beyond the pilot holes were discarded; and (ii) the data in the region where the Cut-2 meets Cut-1 in the 4-Cut configuration (4 mm < X > 11 mm) and the data where Cut-5 meets Cut-2 in the 5-Cut configuration (19 mm < X > 21 mm) were removed and replaced by interpolated data. The refined dataset for the 4-Cut and 5-Cut contour measurements are shown alongside unrefined data in Figs. 6d and 6e, respectively.

When comparing the simulations with the experimental results, it is evident that observed OoPD discontinuities exist in the material ligaments located beyond the pilot holes that are also predicted in the numerical simulations. Similarly, observed discontinuities in the OoPD profile in the region where the Cut-2 meets Cut-1 for the 4-Cut configuration and where Cut-5 meets Cut-2

in the 5-Cut configuration are captured in the simulations; however, the magnitude of these measured discontinuities do not agree with predicted values. This discrepancy is most likely caused by the inaccuracies in the weld simulation used to provide the original (pre-cut) WRS for the cutting simulations (Fig. 5h), and simplifications in the FE cutting simulations themselves (e.g. the omission of finger clamps and sacrificial layers). Nevertheless, the present contour cutting simulations capture the general OoPD profile, implying a realistic prediction CIP contribution.

The post-processed OoPD measurement data were then used in the elastic WRS back-calculation using the following material parameters: E = 195.6 GPa; ν = 0.29. A fully-elastic 3D FE model was generated using the specimen perimeter measurements and meshed using linear hexahedral elements with reduced integration (ABAQUS designation C3D8R). The element length along the cut surface was 1 mm. The element size was biased away from the cut surface to allow for larger elements away from the region of interest, thus reducing computational expense. Post-processed OoPD measurement data was applied as a boundary condition at the nodes of the cut surface to back-calculate the WRS perpendicular to the plane-of-cut (Z). Figure 8 compares back-calculated longitudinal (Z) WRS as recovered using contour method measurements for the embedded cutting configurations. As with the model predictions shown in Fig. 5, WRS measurements employing the 5-Cut contour method (Fig. 8d) produces a more accurate measurement over the 4-Cut approach (Fig. 8c), when comparing back-calculated longitudinal WRS to the complementary synchrotron diffraction measurements [26] and the FE welding simulations [25] presented in Fig. 2. Looking at the comparison along the B2 and B16 lines (Figs. 8a,b) it is clear that even though the overall WRS profiles are qualitatively captured, a number of quantitative discrepancies exist between the WRS captured using contour measurements, diffraction measurements and numerical simulations. Firstly, the WRS profiles recovered from contour measurements are asymmetric, while those measured using diffraction techniques and predicted from the FE welding simulation are symmetric. This discrepancy is a result of the cutting process asymmetry, which leads to a higher amount of CIP in the first half of the cut when the WRS are still high (see Figs. 5,7). Quantitative agreement between contour measurements and the complementary WRS datasets improves as the cut progresses, due to WRS relaxation up to the point that they no longer cause significant yielding of material at the cut tip. Hence, the OoPD is less affected by contribution from CIP in the second half of the cut and the back-calculated WRS are more accurate.

7. Conclusions

The present work examines optimal cutting configurations for the measurement of WRS in a multi-pass austenitic slot weld sample (NeT TG4) using the contour method. Numerical analyses are conducted to examine key features inherent to the cutting process. Stress intensity factor (SIF) analysis is first used as a screening tool to confirm whether or not novel double-embedded cutting configurations (4-Cut, 5-Cut) are more effective than a conventional single-cut (1-Cut) configuration in limiting the effect of CIP on OoPD along the plane-of-cut, thus improving the accuracy of the contour method.

A notable reduction in K_I extrema indicates the WRS redistribution that occurs during a double-embedded cut is less likely to cause plasticity near the cut tip as it progresses through the specimen, thereby improving the accuracy of the contour method for WRS measurement. This improvement is confirmed using three-dimensional FE cutting simulations, which allow direct comparisons of CIP for each cutting configuration. The simulations also reveal significant localisation of CIP in the material ligaments formed between the pilot holes and the outer edges of the specimen when using double-embedded contour cutting configurations. The plasticity in these material ligaments is caused by the WRS redistribution during the cutting process. This

ligament plasticity causes an overall relaxation of internal stresses, thus reducing the likelihood of CIP along the moving cut tip. In contrast, when employing the 1-Cut configuration, CIP accumulates along the first half of the cut that leads to significant asymmetry of the back-calculated WRS along the plane-of-cut.

Overall, the 4-Cut and 5-Cut embedded configurations perform somewhat similar, however it is clear that removal of the outer material ligaments before cutting through the weld region relaxes the high tensile WRS in its vicinity, leading to a lower likelihood of CIP at the moving cut tip when cutting through this region at later stage of the contour cutting – and thus, higher accuracy of the back-calculated WRS across the region of interest. *In general, any successful cutting strategy for contour measurement should delay cutting through the region of interest if it contains significant internal stresses, until these stresses are relaxed via release of the equilibrating stresses found outside the region of interest.* It is clear from present results that the localisation of CIP occurs near the end of the final cut of the 4-Cut configuration, which is undesirable since this region lies adjacent to the weld region. In contrast, the 5-Cut configuration – which first removes the equilibrating outer material ligaments before sectioning the weld region – reduces the tensile WRS across the weld region prior to sectioning, thereby limiting CIP and improving contour measurement accuracy.

All numerical results are validated against a series of WRS measurements performed using the contour method and the cutting configurations of interest. Cutting was performed on a series of benchmark weld specimens produced under the auspices of NeT TG4; as such, the specimens were previously subjected to rigorous examination, including repeat measurement of WRS using complementary neutron and synchrotron diffraction techniques. Agreement between numerical results, diffraction data and the recovered longitudinal WRS profiles obtained using the contour method were established.

Acknowledgements

Residual stress measurements and weld simulations produced under the auspices of the NeT programme via Task Group 4 have significantly advanced best-practice guidelines for treatment of WRS and post-weld plastic strain, adding considerable value to the present work. The authors are also grateful for insightful discussions regarding computational weld mechanics with Prof. M.C. Smith (University of Manchester).

References

[1] P.J. Withers. Residual stress and its role in failure Reports on Progress in Physics 70 (2007) 2211-2264.

[2] M.B. Prime, A.T. DeWald. The Contour Method. in: Schajer GS, (Ed.). Practical Residual Stress Measurement Methods. John Wiley & Sons, Ltd., Chichester,WestSussex, UK, 2013.

[3] M.R. Hill. The Slitting Method. in: Schajer GS, (Ed.). Practical Residual Stress Measurement Methods. John Wiley & Sons, Ltd, 2013. pp. 89-108.

[4] D.J. Smith. Deep Hole Drilling. in: Schajer GS, (Ed.). Practical Residual Stress Measurement Methods. John Wiley & Sons, Ltd, 2013. pp. 65-87.

[5] M.D. Olson, M.R. Hill. A New Mechanical Method for Biaxial Residual Stress Mapping, Experimental Mechanics 55 (2015) 1139-1150.

[6] P. Pagliaro, M.B. Prime, J.S. Robinson, B. Clausen, H. Swenson, M. Steinzig, B. Zuccarello. Measuring Inaccessible Residual Stresses Using Multiple Methods and Superposition, Experimental Mechanics 51 (2011) 1123-1134.

[7] G.S. Schajer. Practical Residual Stress Measurement Methods, John Wiley & Sons Ltd., 2013.

[8] M.B. Prime. Cross-Sectional Mapping of Residual Stresses by Measuring

the Surface Contour after a Cut, Journal of Engineering Materials and Technology (2001) 162-168.

[9] M.B. Prime, R.J. Sebring, J.M. Edwards, D.J. Hughes, P.J. Webster. Laser Surface-Contouring and Spline Data-Smoothing for Residual Stress Measurement, Experimental Mechanics 44 (2004) 176 - 184.

[10] M.R. Hill, M.D. Olson. Repeatability of the Contour Method for Residual Stress Measurement, Experimental Mechanics 54 (2014) 1269-1277.

[11] H.F. Bueckner. Field Singularities and Related Integral Representations, Mechanics of Fracture G.C. Sih, ed. (1973) 239-314.

[12] M.B. Prime, A.L. Kastengren. The Contour Method Cutting Assumption: Error Minimization and Correction. Proceedings of the SEM Annual Conference. Indianapolis, Indiana, USA: Society for Experimental Mechanics Inc., 2010.

[13] F. Hosseinzadeh, J. Kowal, P.J. Bouchard. Towards good practice guidelines for the contour method of residual stress measurement, The Journal of Engineering (2014).

[14] F. Hosseinzadeh, P. Ledgard, P.J. Bouchard. Controlling the Cut in Contour Residual Stress Measurements of Electron Beam Welded Ti-6Al-4V Alloy Plates, Experimental Mechanics 53 (2013) 829-839.

[15] L. Hacini, N. Van Lê, P. Bocher. Evaluation of Residual Stresses Induced by Robotized Hammer Peening by the Contour Method, Experimental Mechanics 49 (2009) 775-783.

[16] P.G. Frankel, P.J. Withers, M. Preuss, H.T. Wang, J. Tong, D. Rugg. Residual stress fields after FOD impact on flat and aerofoil-shaped leading edges, Mechanics of Materials 55 (2012) 130-145.

[17] P. Pagliaro, M.B. Prime, B. Clausen, M.L. Lovato, B. Zuccarello. Known Residual Stress Specimens Using Opposed Indentation, Journal of Engineering Materials and Technology 131 (2009) 031002.

[18] A.T. DeWald, M.R. Hill. Eigenstrain based model for prediction of laser peening residual stresses in arbitrary 3D bodies. Part 2: model verification, Journal of Strain Analysis for Engineering Design 44 (2009) 13-27.

[19] R. Kaiser, M. Stefenelli, T. Hatzenbichler, T. Antretter, M. Hofmann, J. Keckes, B. Buchmayr. Experimental characterization and modelling of triaxial residual stresses in straightened railway rails, The Journal of Strain Analysis for Engineering Design 50 (2015) 190-198.

[20] B. Ahmad, M.E. Fitzpatrick. Residual Stresses in Ultrasonically Peened Fillet Welded Joints, Advanced Materials Research 996 (2014) 755-760.

[21] S.H. Shin. FEM analysis of plasticity-induced error on measurement of welding residual stress by the contour method, Journal of Mechanical Science and Technology 19 (2005) 1885-1890.

[22] R.J. Dennis, D.P. Bray, N.A. Leggatt, M. Turski. Assessment of the influence of plasticity and constraint on measured residual stresses using the contour method. ASME Pressure Vessels and Piping Division Conference, vol. Volume 6: Materials and Fabrication, Parts A and B. Chicago, IL, USA: ASME, 2008. p.477-485.

[23] Y. Traoré, F. Hosseinzadeh, P.J. Bouchard. Plasticity in the Contour Method of Residual Stress Measurement, Advanced Materials Research 996 (2014) 337-342.

[24] A.H. Mahmoudi, A.R. Hosseinzadeh, M. Jooya. Plasticity effect on residual stresses measurement using contour method, International Journal of Engineering-Transactions A: Basics 26 (2013) 1203-1212.

[25] O. Muránsky, M.C. Smith, P.J. Bendeich, T.M. Holden, V. Luzin, R.V. Martins, L. Edwards. Comprehensive numerical analysis of a three-pass bead-in-slot weld and its critical validation using neutron and synchrotron diffraction residual stress measurements, International Journal of Solids and Structures 49 (2012) 1045-1062.

[26] R.V. Martins, C. Ohms, K. Decroos. Full 3D spatially resolved mapping of residual strain in a 316L austenitic stainless steel weld specimen, Materials Science and Engineering: A 527 (2010) 4779-4787.

[27] M.T. Hutchings, P.J. Withers, T.M. Holden, T. Lorentzen. Introduction to the Characterization of Residual Stress by Neutron Diffraction, CRC Press, 2005.

[28] E. Kröner. Zeitschrift Fur Physik 151 (1958) 504-518.

[29] R.V. Martins, Honkimäki. Texture, Stress, and Microstructure 35 (2003) 145-152.

[30] R.V. Martins. NeT - Task Group 4: Three-Pass Slot Wled Specimen in Austenitic Stainless Steel. Protoc for the Destructive and Non-Destructive Determination of Residaul Stress in Three-Pass Slot Weld Specimens in Austenitic Stainless Steel, Network on Neutorn Techniques Standardisation for Structural Integrity Report Version 3.3. NeT - Task Group 4: Three-Pass Slot Wled Specimen in Austenitic Stainless Steel. Protoc for the Destructive and Non-Destructive Determination of Residaul Stress in Three-Pass Slot Weld Specimens in Austenitic Stainless Steel, Network on Neutorn Techniques Standardisation for Structural Integrity Report Version 3.3, 2009.

[31] O. Muránsky, C.J. Hamelin, M.C. Smith, P.J. Bendeich, L. Edwards. The effect of plasticity theory on predicted residual stress fields in numerical weld analyses, Computational Materials Science 54 (2012) 125-134.

[32] O. Muránsky, M.C. Smith, P.J. Bendeich, L. Edwards. Validated numerical analysis of residual stresses in Safety Relief Valve (SRV) nozzle mock-ups, Computational Materials Science 50 (2011) 2203-2215.

[33] D. Systèmes. Abaqus. 2013.

[34] R.M. Smith. FEAT-WMT: FEAT-WMT: Weld-Modelling Tool User Guide: FeatPlus Limited, 2010.

[35] J. Lemaitre, J.-L. Chaboche. Mechanics of Solid Materials, Cambridge University Press, 1994.

[36] O. Muránsky, C.J. Hamelin, V.I. Patel, V. Luzin, C. Braham. The influence of constitutive material models on accumulated plastic strain in finite element weld analyses, International Journal of Solids and Structures 69–70 (2015) 518-530.

[37] ABAQUS. A Novel Approach to Annealing using ABAQUS - behaviour with soft annealing. SIMULIA, 2007. p.A Novel Approach to Annealing using ABAQUS - behaviour with soft annealing.

[38] F. Hosseinzadeh, Y. Traore, P.J. Bouchard, O. Muránsky. Mitigating Cutting-Induced Plasticity in the Contour Method, Part 1: Experimental, International Journal of Solids and Structures (2016).

[39] O. Muránsky, C.J. Hamelin, F. Hosseinzadeh, M.B. Prime. Mitigating Cutting-Induced Plasticity in the Contour Method, Part 2: Numerical Analysis, International Journal of Solids and Structures (2016).

[40] Y. Traore. Controlling plasticity in the contour method of residual stress measurement. DDEM, vol. PhD. Milton Keynes: The Open University, 2013.

[41] Y. Traore, P.J. Bouchard, J. Francis, F. Hosseinzadeh. A Novel Cutting Strategy for Reducing Plasticity Induced Errors in Residual Stress Measurements Made With the Contour Method, ASME Conference Proceedings 2011 (2011) 1201-1212.

[42] M.B. Prime. Plasticity effects in incremental slitting measurement of residual stresses, Engineering Fracture Mechanics 77 (2010) 1552-1566.

[43] I.T. 21432:2005. Non-destructive testing-standard test method for determining residual stresses by neutron diffraction. 2005.

[44] O. Muránsky, C.J. Hamelin, F. Hosseinzadeh, M.B. Prime. Mitigating Cutting-Induced Plasticity in the Contour Method, Part 2: Numerical Analysis, International Journal of Solids and Structures submitted to the journal (2016).

[45] M.B. Prime, A.T. DeWald. The Contour Method. in: Schajer GS, (Ed.). Practical Residual Stress Measurement Methods. 2013. pp. 109-138.

[46] M.B. Prime, R.J. Sebring, J.M. Edwards, D.J. Hughes, P.J. Webster. Laser Surface-contouring and Spline Data-smoothing for Residual Stress Measurement, Society for Experimental Mechanics 44 (2004) 176.

Appendix

Considerable advantage can be made of the self-constraining nature of double-embedded cuts for reducing the influence of CIP across the region of interest (in the present example, the weld region). It has been shown that the material ligaments formed between the pilot holes and the outer edges of the specimen mitigate CIP when cutting progresses across the weld region. This mitigation occurs due to two processes:

1. The ligaments act as self-constraint, allowing a portion of the WRS to be redistributed into the ligament and away from the cut tip. The ligament thus limits *short-range* stress intensification near the cut tip (and consequently, CIP). The ligaments are not rigid; the material will behave in an elasto-plastic manner.
2. Once local stresses in the ligament exceed the material yield strength, this ligament will deform plastically. In the case of our weldment, compressive equilibrating stresses near the outer edge of the specimen lead to compressive plasticity. This bulk compression leads to a relaxation of the overall, *long-range* tensile stresses in the weld region, hence to a lower likelihood of CIP when cutting through the weld region at a later stage of the cutting procedure.

It is thus important that these material ligaments are stiff enough to provide self-constraint for the specimen during cutting (to limit short-range stress intensification), but simultaneously they need to be compliant enough to generate compressive plasticity (leading to long-range stress relaxation). The strength of these material ligaments is dictated by the ligament size, as determined by the position of the pilot holes from the outer edge of the specimen. If these holes are placed too far from the outer edges of the specimen, self-constraint is assured but the analyst will no longer benefit from long-range stress relaxation. Conversely, if the holes are placed too close to the outer edges, the ligaments formed will not provide sufficient self-constraint for the specimen during the cutting process and significant short-range stress redistribution results, leading again to a higher likelihood of CIP along the moving cut tip. It follows that a means of optimising pilot hole location is necessary to identify the ideal trade-off between these two competing effects.

The FE model developed to simulate the 4-Cut process was modified to examine the effect of different pilot hole locations. Apart from these locations, the 4-Cut procedure as shown in Fig. 3b remained identical. Figure A1 presents the elasto-plastic OoPD profile extracted from nodal points along the FE model plane-of-cut from four different analyses. These analyses comprise pilot holes located the following distances from the outer sample edges: (Fig. A1a) 5 mm; (Fig. A1b) 1 mm; (Fig. A1c) 10 mm; and (Fig. A1d) 20 mm. Each profile is presented alongside an idealised elastic OoPD profile, which was extracted from a fully elastic FE analysis and does not contain CIP. It is clear that using pilot holes at distance greater than 5 mm from the outer edge of the specimen limits the amount of CIP accumulated in the outer material ligaments, thereby limiting WRS relaxation near the weld region and causing significant CIP along the moving cut tip when the highly tensile region is sectioned. The effect of CIP is manifested by a greater deviation of elasto-plastic OoPD profile form the fully elastic OoPD profile across the weld region. In contrast, pilot holes inserted less than 5 mm from the outer specimen edges lead to ligaments that cannot provide sufficient restraint. CIP continuously accumulates along the moving cut tip as a result, particularly during the first half of the cut as one would expect in a conventional cutting approach (i.e. no pilot holes and external clamping). Based on this analysis, pilot holes located 5 mm from the outer sample edge were selected for the double-embedded configurations studied in the present work.

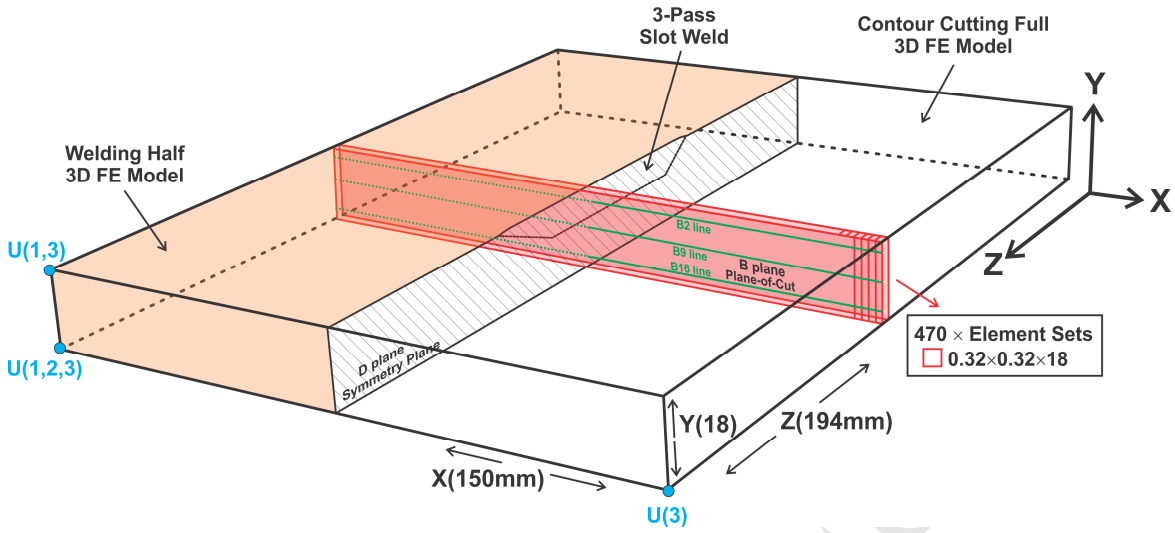

Fig. 1: Schematic of the NeT TG4 benchmark specimen, and its representation for numerical FE analyses (X = transverse direction, Y = normal direction, Z = longitudinal direction). The FE welding analysis used a half-model (highlighted), taking advantage of process symmetry. The FE cutting analysis must use a full model due to asymmetry about the weld centreline in the cutting process. Planar sectioning of the model is performed along the plane-of-cut, which is comprised of a series of element sets that are progressively removed to simulate the cutting process. In cases where clamping is not used, a set of pin constraints (blue dots in the figure) are applied to the model to prevent rigid body rotation; U() defines the direction of nodal constraint (1,2,3=X,Y,Z).

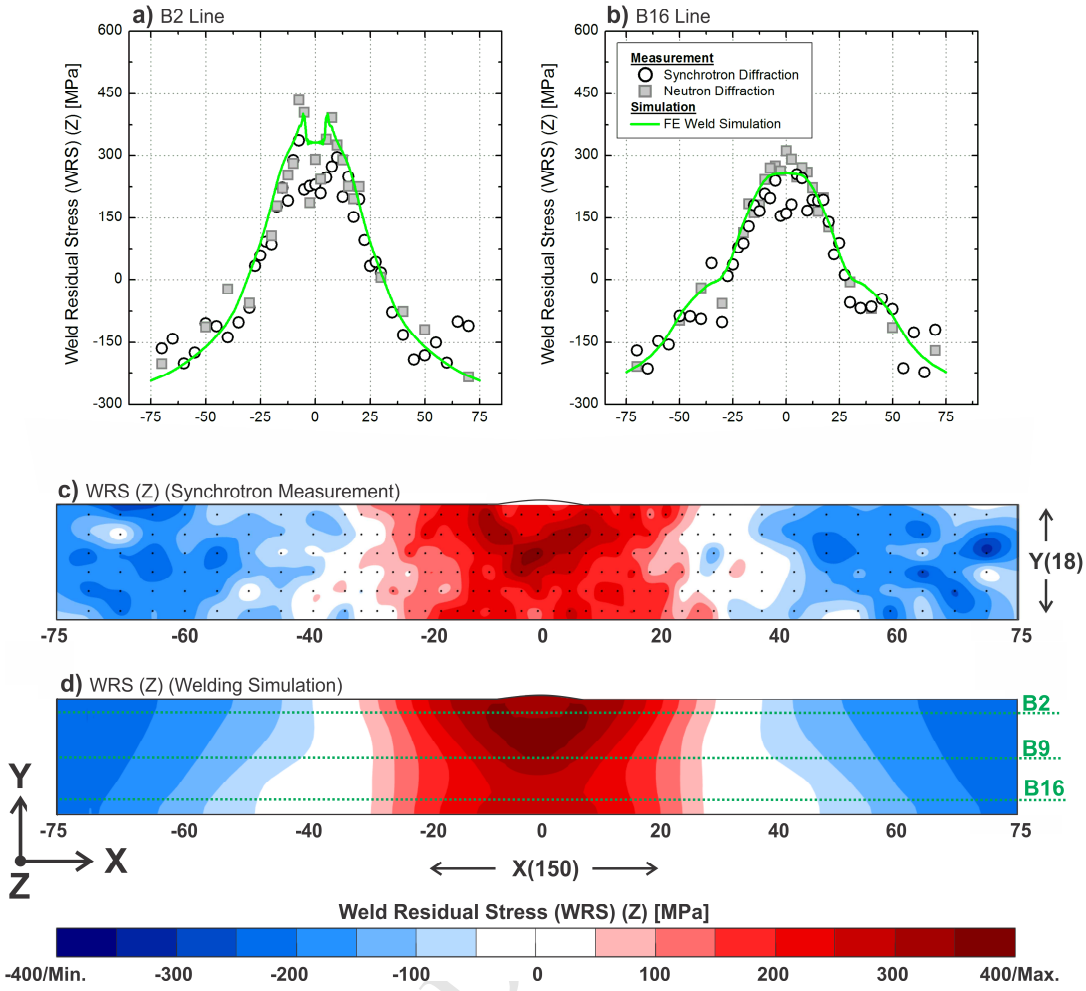

Fig. 2: Longitudinal WRS distribution along the plane-of-cut for the NeT TG4 benchmark weld specimen. Cross-weld stress profiles are shown alone Line B2 (a) and Line B16 (b), located 2 mm and 16 mm below the top surface of the specimen, respectively. For synchrotron diffraction measurements (c) and FE model predictions (d), the profiles were extracted from WRS contours obtained along the plane-of-cut and presented alongside neutron diffraction measurements.

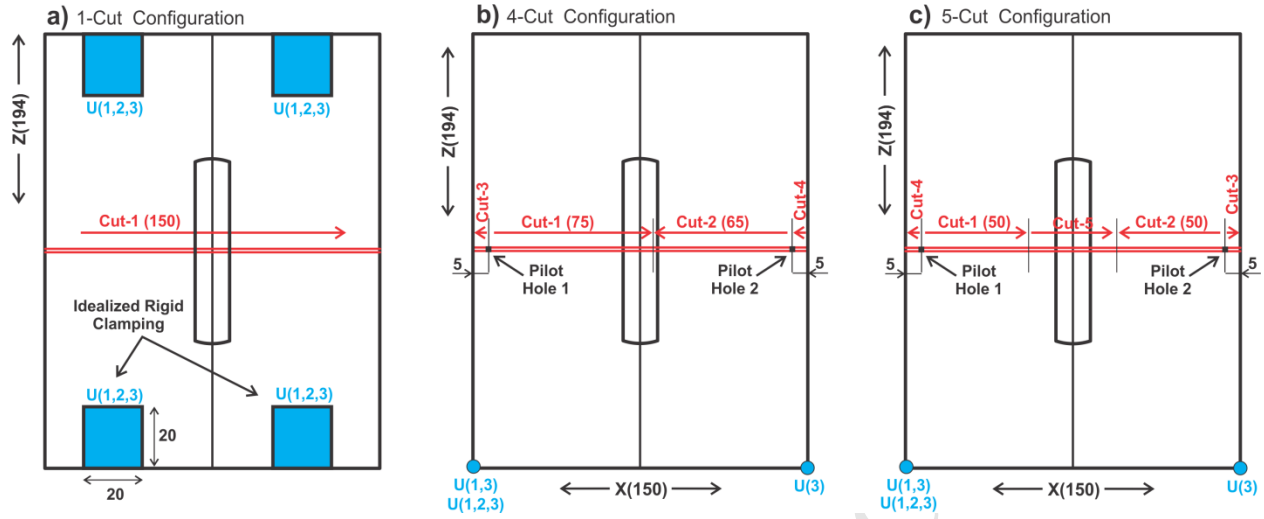

Fig. 3: Schematic diagrams outlining the FE representation of the cutting configurations under investigation: (a) conventional (1-Cut) configuration with external (clamping) constraint; and (b) 4-Cut and (c) 5-Cut double-embedded cutting configurations, which use two pilot holes for self-constraint and only light clamping to prevent rigid body motion.

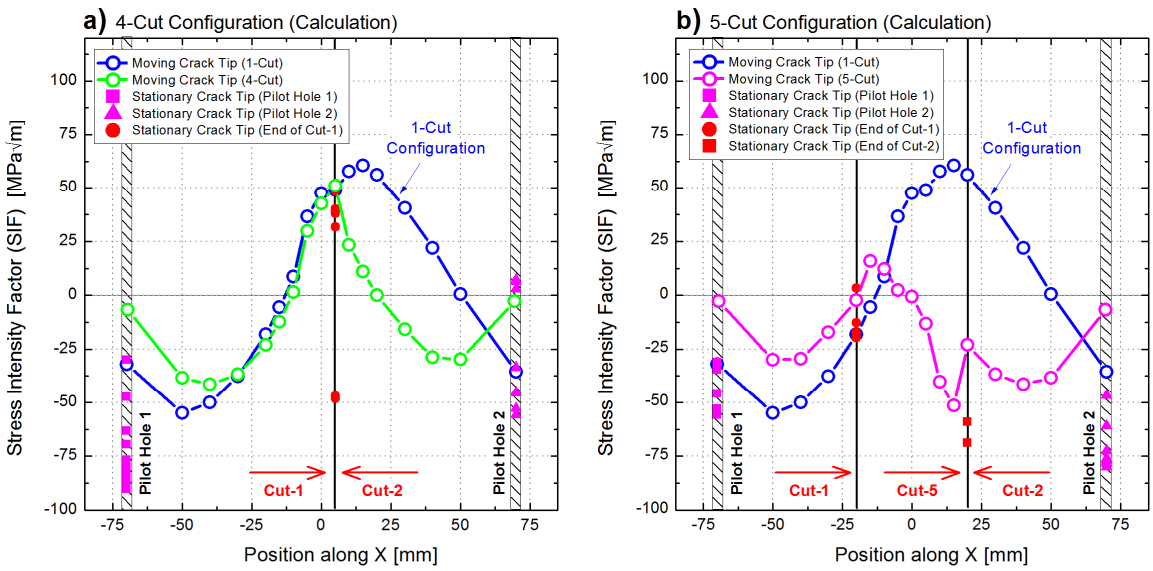

Fig. 4: Stress intensity factor (SIF) distributions obtained using a 2D elastic FE analysis containing the neutron-diffraction measured WRS distribution along Line B2 (Fig. 2a). The SIF distribution for the 1-Cut configuration is compared to that obtained for 4-Cut (a) and 5-Cut (b) configurations.

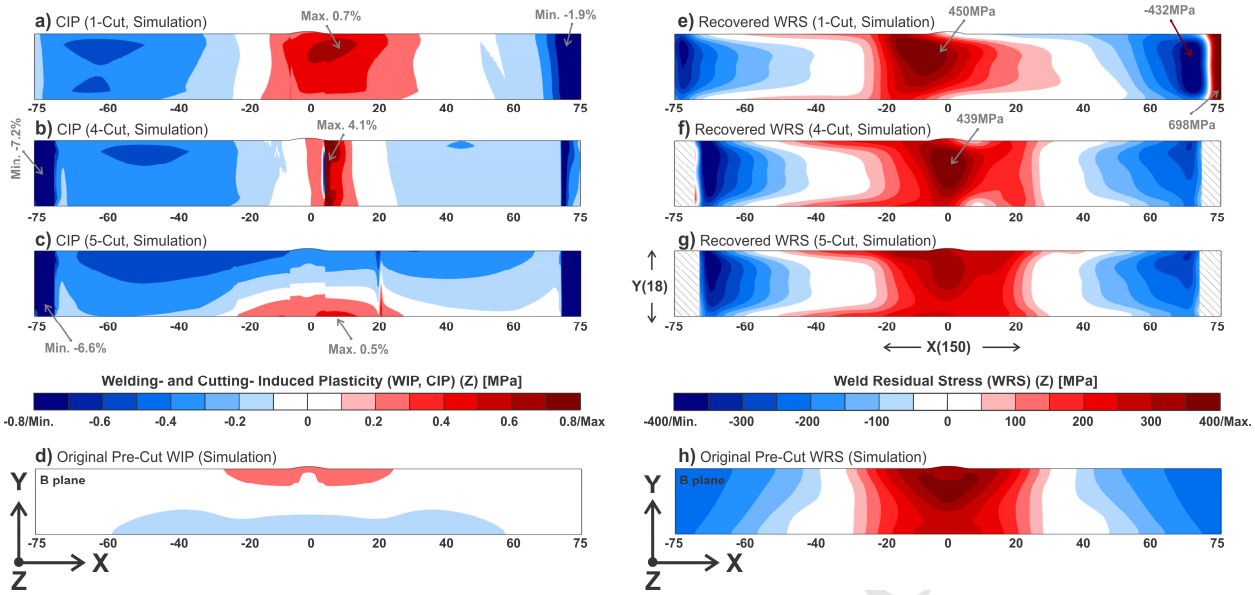

Fig. 5: Contour plots of the predicted longitudinal component of CIP (a-c) and the resultant back-calculated WRS (e-g) for the following configurations: (a,e) 1-Cut; (b,f) 4-Cut; and (c,g) 5-Cut. Numerical solutions are compared to the original, pre-cut WIP (d) and WRS (h) used for the NeT TG4 benchmark weld specimen.

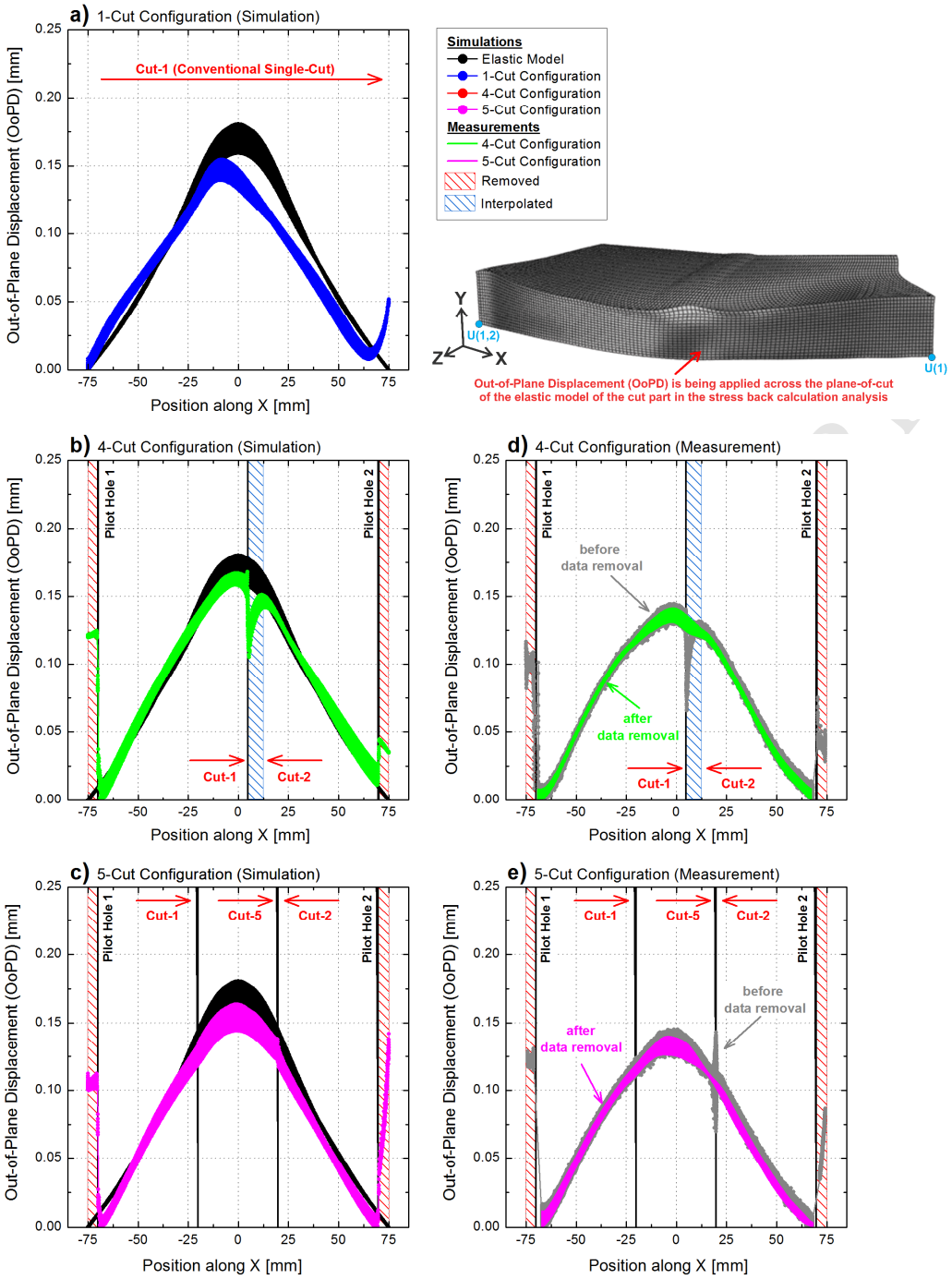

Fig. 6: Out-of-plane displacement (OoPD) profiles for (a) 1-Cut, (b,d) 4-Cut and (c,e) 5-Cut configurations. For the double-embedded configurations, both model predictions (b,c) and experimental contour measurements (d,e) are presented. For all simulation results, the predicted OoPD from the elasto-plastic FE models are presented alongside the idealised OoPD profile (shown in black) obtained using a fully elastic FE model that does not account for CIP.

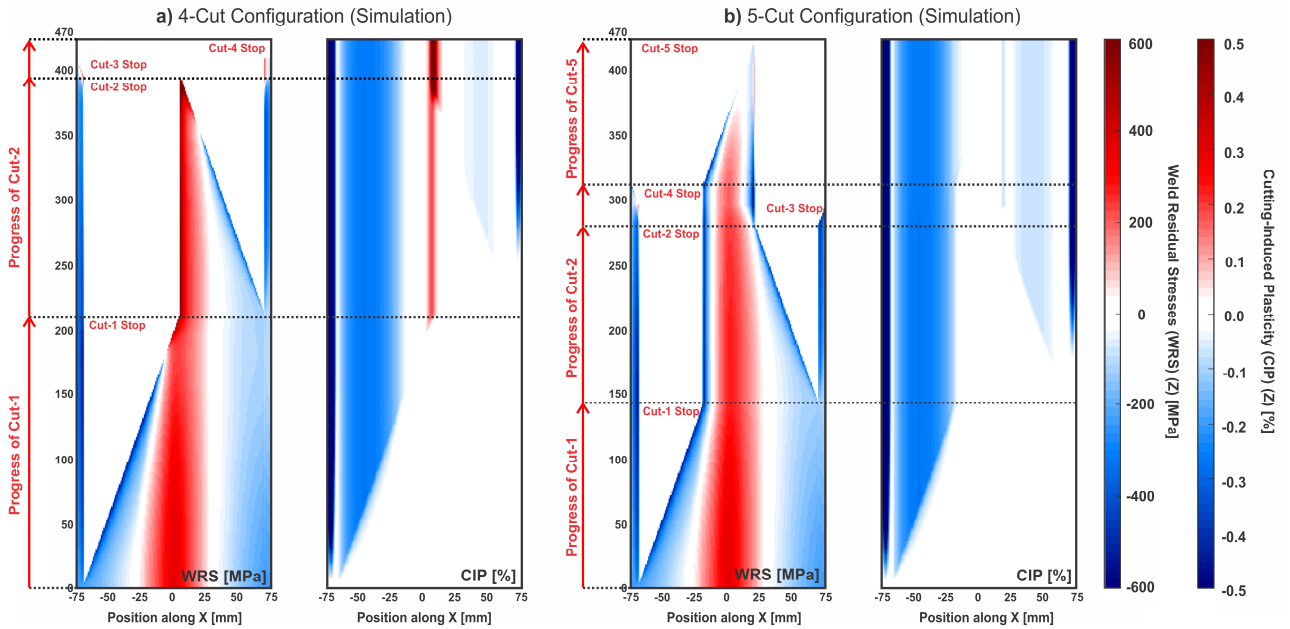

Fig. 7: The transient redistribution of WRS and development of CIP for 4-Cut (a) and 5-Cut (b) simulations. Predictions are taken along Line B9 (Fig. 1). The ordinate axis refers to the number of element sets (from the total of 470) removed. The stop points of each cut are identified for each simulation, allowing the analyst to observe the evolution of WRS and CIP at all points during the cutting procedure.

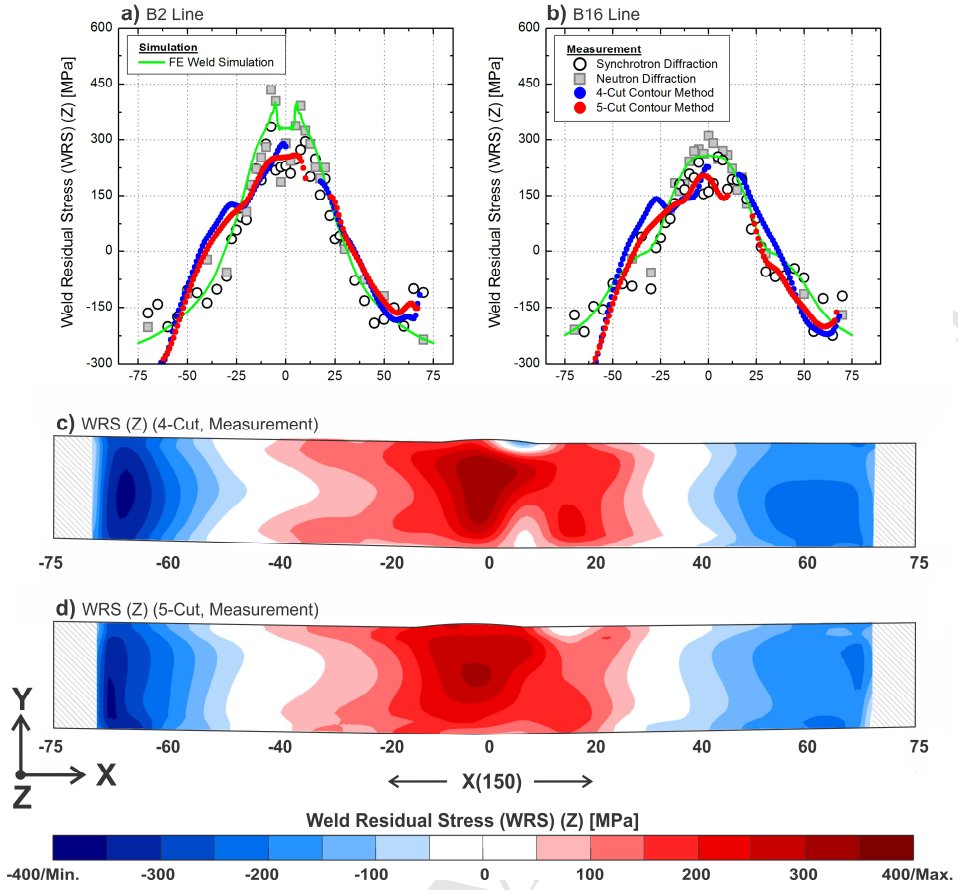

Fig. 8: Experimental contour measurements, extracted from two NeT TG4 benchmark weld specimens subjected to 4-Cut and 5-Cut double-embedded cutting configurations. Longitudinal WRS profiles along Line B2 (a) and Line B16 (b), recovered using the contour method, are compared against numerical predictions and diffraction measurements of the original (pre-cut) WRS profiles (Figs. 2a,b). Contour plots of the back-calculated WRS distribution along the plane-of-cut for both the 4-Cut (c) and 5-Cut (d) configuration are also shown.

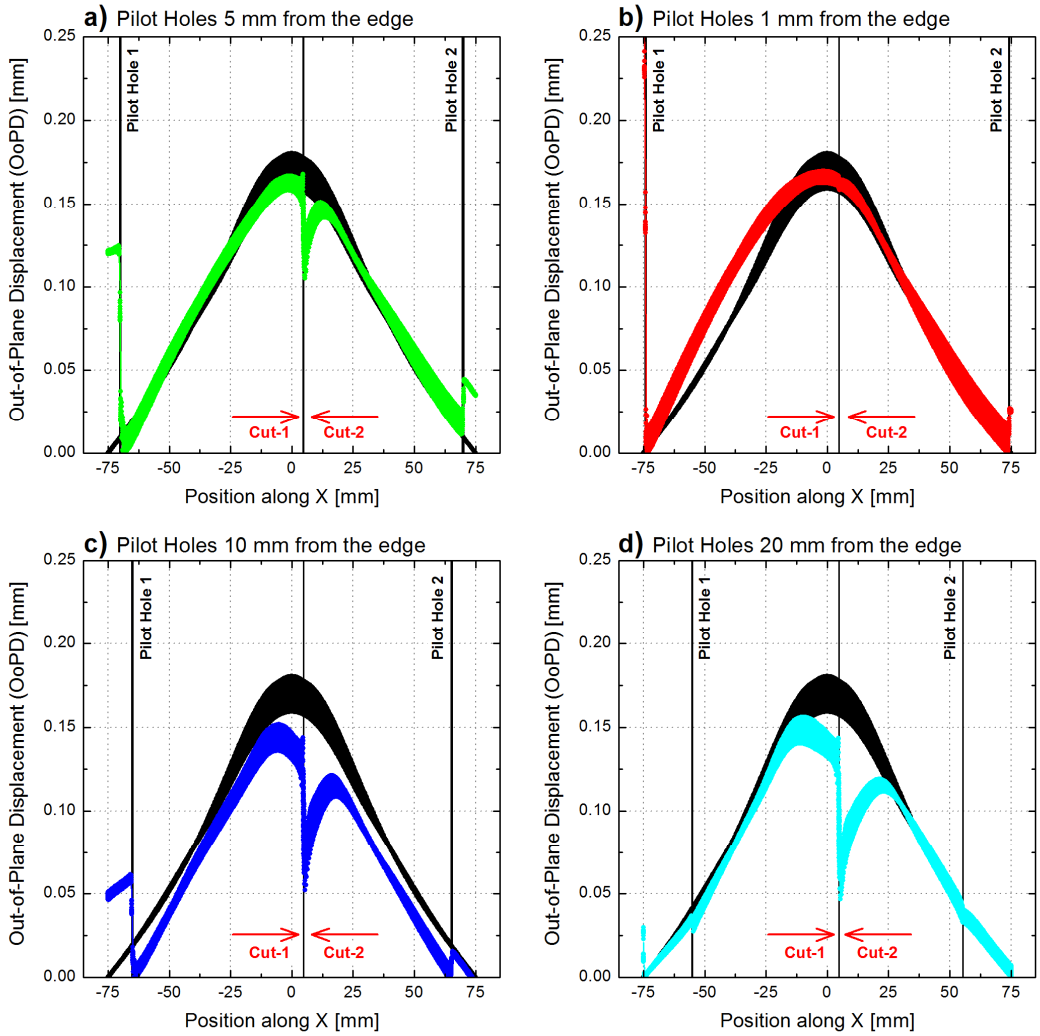

Fig. A1: Out-of-plane displacement (OoPD) data extracted from the 4-Cut FE cutting simulation, performed using different pilot hole distances from the outer sample edges: (a) 5 mm; (b) 1 mm; (c) 10 mm; and (d) 20 mm. Results from the elasto-plastic FE simulations (in colour) are presented alongside idealised OoPD profiles from a fully elastic FE simulation (in black), which does not contain the influence of CIP.

- The cutting process of the contour method was simulated via finite element analysis
- Several cutting strategies were examined to minimise cutting-induced plasticity
- Cutting strategies were varied through clamping and cutting direction/orientation
- A double-embedded cutting strategy produced the lowest measurement error
- For welded specimens, sectioning should be performed through the weld region last